Supporting Information

Two-dimensional lead-free silver-bismuth double perovskite nanobelts with intrinsic chirality via co-antisolvent modulation strategy

Xuexia Yu,[a] Rong Lu,[a] Pengfei Zhang,[a] Shun Wang,[a,b] Yihuang Chen,*[a,b] Shuang Pan*[a,b]

[a] College of Chemistry and Materials Engineering, Wenzhou University, Wenzhou 325035, China.

E-mail: yhchen@wzu.edu.cn; shuangpan@wzu.edu.cn.

[b] Institute of New Materials and Industrial Technologies, Wenzhou University, Wenzhou 325035, China.

Materials and methods

Materials

(*R*)-(+)-β-Methylphenethylamine (*R*-MPEA, 99%), bismuth bromide ($BiBr_3$, >99%), bismuth iodide (BiI_3, >99%), silver bromide (AgBr, 99.9%), silver iodide (AgI, >99%) were purchased from Macklin. Hydrobromic acid (HBr, 48 wt% in H_2O, ≥99.99%), hydroiodic acid (HI, 57 wt% in H_2O, ≥99.99%), oleylamine (OAm, 70%) and *N, N*-Dimethylmethanamide (DMF, 99.8 %, extra dry) were purchased from Aladdin. Toluene (TOL, anhydrous, 99.8%), diethyl ether (≥99.5%), tetrahydrofuran (≥99%), ethyl Acetate (≥99.5%), dichloromethane (≥99.7%), ethanol (≥95.0%), chloroform (CF, ≥99.5%), dichloromethane (≥99%) were purchased from Sinopharm Chemical Reagent Co., Ltd. All materials for synthesis were used without further purification.

Synthesis of 2D lead-free Hybrid Double Perovskite (*R*-MPEA)$_4$AgBiBr$_{8-8x}$I$_{8x}$ colloidal solution

Prior to the synthesis of 2D lead-free hybrid double perovskite (*R*-MPEA)$_4$AgBiBr$_{8-8x}$I$_{8x}$, the precursor salts (i.e., *R*-MPEABr and *R*-MPEAI) were synthesized based on previous report.[1] Taking (*R*-MPEA)$_4$AgBiBr$_8$ NBs as an example, *R*-MPEABr (107.5 mg, 0.5 mmol), $BiBr_3$ (23.5 mg, 0.125 mmol) and AgBr (56.2 mg, 0.125 mmol) were dissolved in the mixture of DMF (0.5 mL) and OAm (1.2 μL) to prepare the precursor solution. 5 μL of the precursor solution was rapidly injected into a 5 mL co-antisolvent mixture, consisting of 2 mL of chloroform and 3 mL of toluene, while vigorously stirring the solution for duration of 2 minutes. Finally, a yellow colloidal solution was obtained. The synthesis of (*R*-MPEA)$_4$AgBiBr$_{8-8x}$I$_{8x}$ was conducted following a similar procedure as the synthesis of (*R*-MPEA)$_4$AgBiBr$_8$. Detailed precursor amounts used for the synthesis are presented in **Table S1**.

Table S1. Parameters of synthesis of **(*R*-MPEA)$_4$AgBiBr$_{8-8x}$I$_{8x}$** with different content of iodine.

***x* (%)**	***R*-MPEABr (mmol)**	***R*-MPEAI (mmol)**	**AgBr (mmol)**	**$BiBr_3$ (mmol)**	**AgI (mmol)**	**BiI_3 (mmol)**
0	0.5	0	0.125	0.125	0	0
25	0.375	0.125	0.094	0.094	0.031	0.031
50	0.25	0.25	0.063	0.063	0.063	0.063
75	0.125	0.375	0.031	0.031	0.094	0.094
100	0	0.5	0	0	0.125	0.125

Optimizing synthesis of (*R*-MPEA)$_4$AgBiBr$_8$ colloidal with different amount of OAm ligand

To investigate the impact of varying amounts of OAm on the optical properties of (*R*-MPEA)$_4$AgBiBr$_8$ colloidal solution, the volume of OAm was adjusted to 0.5, 1.0, 1.2, 1.5, and 2.0 μL during the synthesis process.

Synthesis of corresponding Bi-base material under the same optimized conditions

The synthesis procedure, similar to that of (*R*-MPEA)$_4$AgBiBr$_8$, with the exception of Ag^+ being absent from the precursor solution, was as follows. Specifically, all experimental conditions of Bi-base material remained the same as those of (*R*-MPEA)$_4$AgBiBr$_8$ except that the precursors were changed to 0.5 mmol of *R*-MPEABr and 0.125 mmol of $BiBr_3$ dissolved in DMF.

Material characterization

Powder X-ray diffraction. Powder X-ray diffractions (XRD) were performed on a Bruker D8 Advance XRD system at emission current of 40 mA and accelerating voltage of 40 mV. The diffraction patterns were collected in the 2θ range of 5−40° with a step

size of 6°/min. Bragg diffraction equation: $2d\sin\theta = m\lambda$ (m = 1, 2, 3···), d is the lattice/ unit constant, θ is the diffraction angle, m is the order and λ = 1.54 Å for Cu K.

Circular dichroism spectrum measurement. The CD and absorbance measurements of the prepared colloid were carried out on Applied Photophysics Chirascan V100 spectrometer with the scanning rate of 200 nm/min, and the data interval was 1 nm. The anisotropy factor of CD absorption (g_{abs}) was calculated as Equation (1).

$$g_{abs} = \text{CD (mdeg)} /(\text{abs}\times 32980) \quad (1)$$

where CD is the value of ellipticity (θ, in mdeg) and abs is the value of UV–vis absorption.[2]

Optical measurements. Photoluminescence (PL) spectra were obtained by a Hitachi 5J1-0004 fluorescence spectrometer with 365 nm xenon lamp excitation. The UV-vis Spectrometer of Shimadzu UV-2600 was applied to acquire UV-vis absorption spectra. Time-Resolved photoluminescence (TRPL) spectra were carried out by a spectrofluorometer (Edinburgh, FLS 980).

Morphological and structural characterization. SEM images were acquired using the FEI field emission electron microscope, Nano Sem 200. AFM images were collected by using a Bruker Dimension icon microscope in the tapping mode. Transmission electron microscopy (TEM) images were collected by using JEOL JEM-2100F microscope at 200 kV accelerating voltage, and EDS elements mapping images were characterized to analysis elements of the samples. The chemical composition on the surface of the particles was analyzed using X-ray photoelectron spectroscopy (XPS) conducted on an ESCALAB 250Xi versa probe spectrometer (analyzer resolution ≤ 0.5 eV) with a monochromatic Al Kα radiation ($h\nu$ = 486.6 eV).

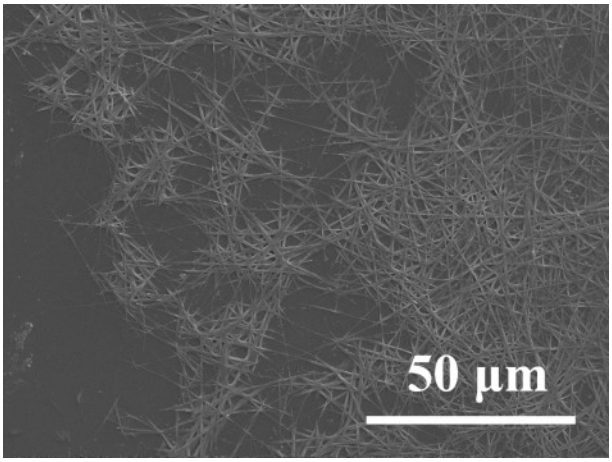

Figure S1. The *large-scale* SEM image of (*R*-MPEA)$_4$AgBiBr$_8$ NBs.

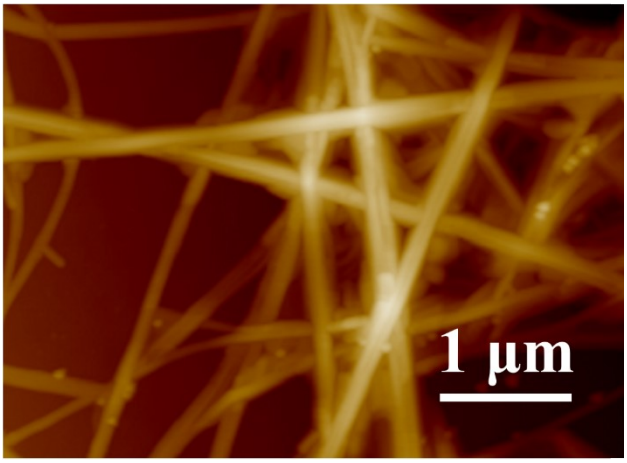

Figure S2. AFM image of the 2D double perovskite (*R*-MPEA)$_4$AgBiBr$_8$ NBs.

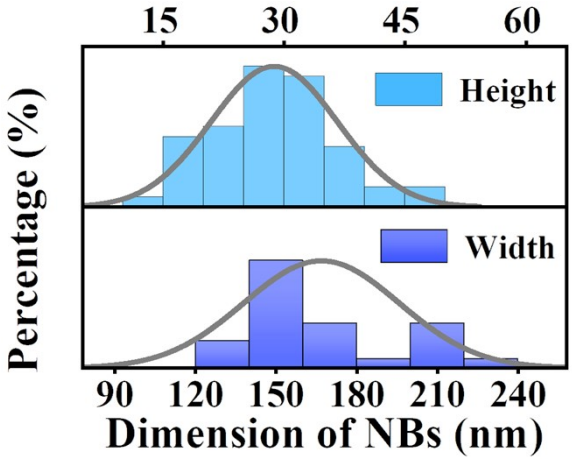

Figure S3. Height and width distribution histogram of the 2D double perovskite (*R*-MPEA)$_4$AgBiBr$_8$ NBs.

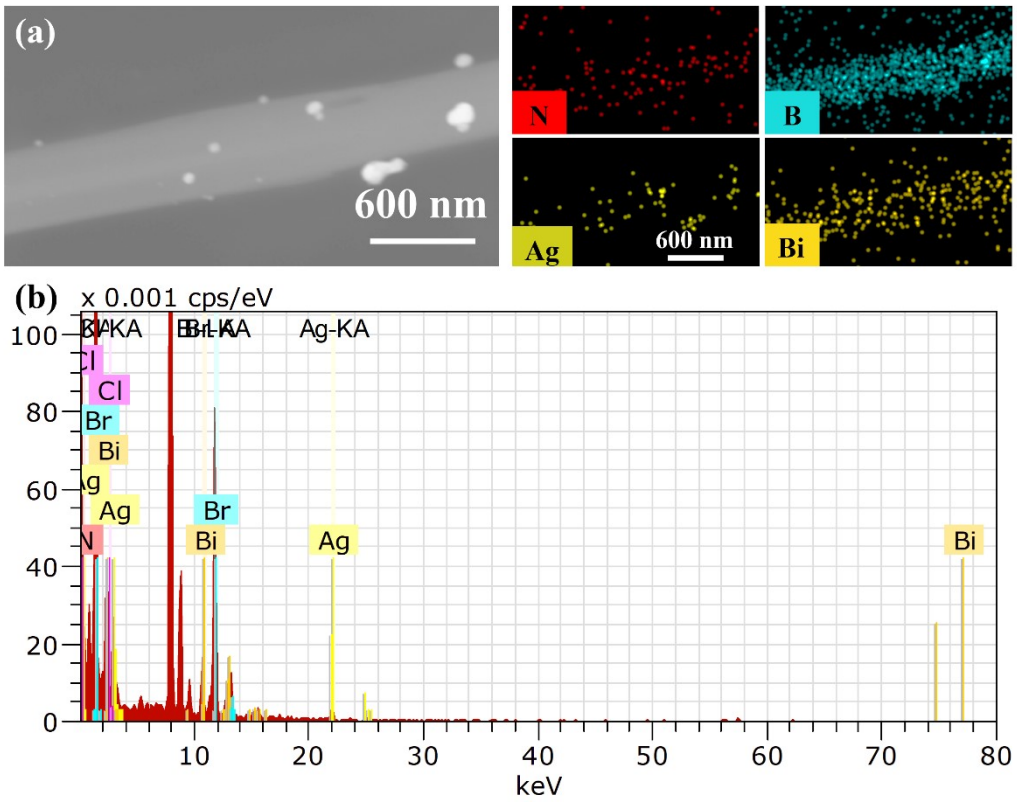

Figure S4. (a) EDS element mapping and (b) EDS spectrum of (*R*-MPEA)$_4$AgBiBr$_8$ NBs.

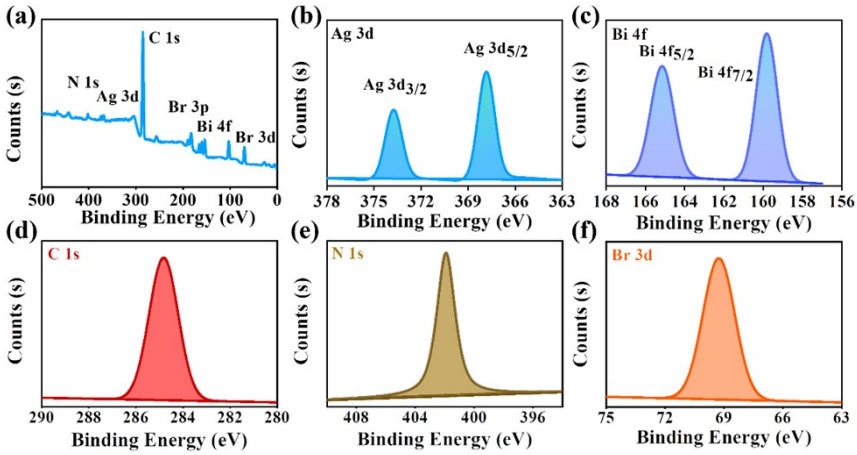

Figure S5. XPS spectra of the (a) survey spectrum, (b) Ag 3d and (c) Bi 4f, (d) C 1s, (e) N 1s and (f) Br 3d of (*R*-MPEA)$_4$AgBiBr$_8$ NBs.

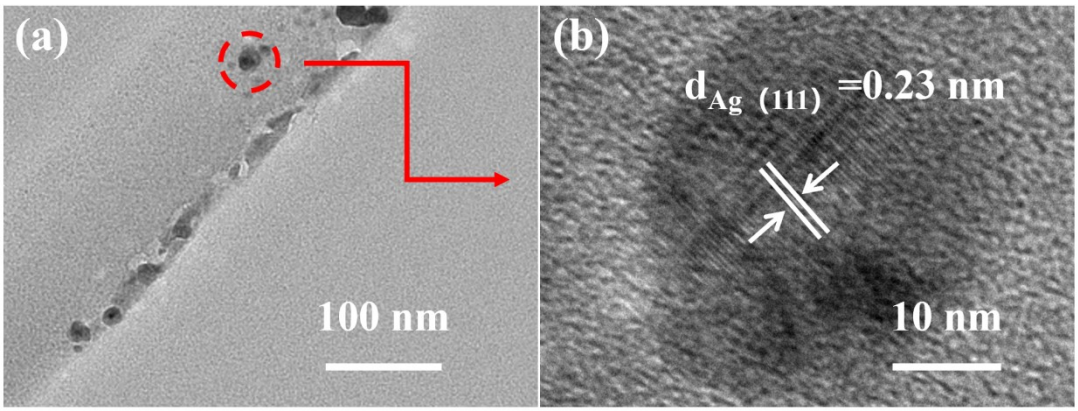

Figure S6. (a) Low resolution TEM and (b) HRTEM micrographs of the black dots on (*R*-MPEA)$_4$AgBiBr$_8$ NBs.

The observed one-dimensional morphology of the (*R*-MPEA)$_4$AgBiBr$_8$ NBs are distinct from that (e.g., microplates[3]) of achiral double perovskite materials in literature. This distinction can likely be attributed to the presence of a polar axis in chiral perovskite nanocrystals due to the addition of moderately polar chloroform, which

governs their preferred growth direction.[1, 4] The differences in growth rates between the polar axis direction and the vertical direction were proposed as the underlying cause of the unique one-dimensional shape observed in the (R-MPEA)$_4$AgBiBr$_8$ NBs. As presented in **Figures S4**, the corresponding energy dispersive X-ray spectroscopy (EDS) diagram and element mapping revealed a homogenous spatial distribution of N, Ag, Bi, Br elements. It is worth noting that the appearance of dark spots observed in NBs (**Figure 1c**) can be ascribed to the formation of metallic silver clusters resulting from the reduction of silver ions by the electron beam during TEM observation.[5] To confirm this point, we conducted high-resolution TEM structural analysis on the dark spots attached to (R-MPEA)$_4$AgBiBr$_8$ NBs. As illustrated in **Figure S6**, these nanodots with higher contrast exhibit distinctive lattice fringes with a lattice spacing of 0.23 nm, corresponding to the (111) spacing of metallic silver. This observation aligns with findings in previously published literature.[6] It has been reported in the literature that the presence of metallic silver nanoparticles can be attributed to the reduction of Ag^+ ions by the electron beam during TEM characterization.[7] Similar occurrences of metal ion reduction have been observed in achiral double perovskite systems.[8] The X-ray photoelectron spectroscopy (XPS) was conducted to provide further confirmation of the valence state and chemical composition of the (R-MPEA)$_4$AgBiBr$_8$ NBs, as depicted in **Figures S5**. Specifically, two peaks corresponding to Ag $3d_{3/2}$ and $3d_{5/2}$ were observed at 373.51 and 367.75 eV, respectively, confirming the presence of Ag^+ in the NBs.[9] Additionally, the presence of Bi^{3+} was supported by the appearance of two peaks at 165.2 (Bi $4f_{5/2}$) and 153.85 eV (Bi $4f_{3/2}$).

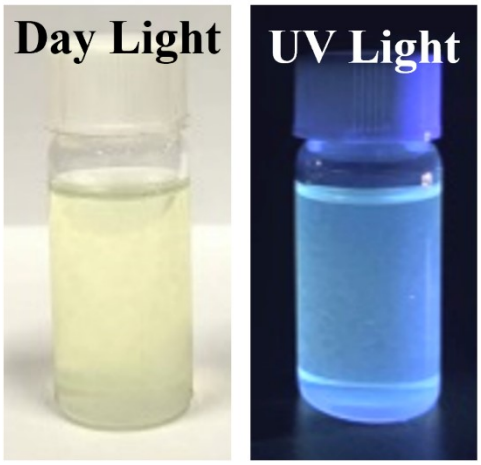

Figure S7. Digital images of (*R*-MPEA)$_4$AgBiBr$_8$ NBs under daylight and UV irradiation, respectively. The images depicted the visual appearance of the (*R*-MPEA)$_4$AgBiBr$_8$ colloidal solution, exhibiting a yellow color when exposed to sunlight and emitting a cyan-colored fluorescence under 365 nm UV light. These findings align with the optical properties observed in other 2D lead-free Ag and Bi-based double perovskites.[3]

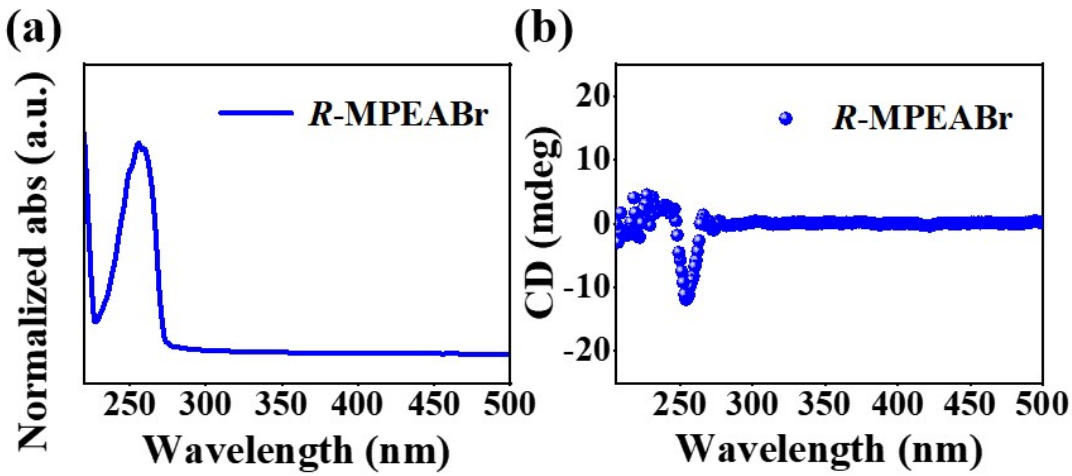

Figure S8. (a) UV and (b) CD Spectrum of *R*-MPEABr.

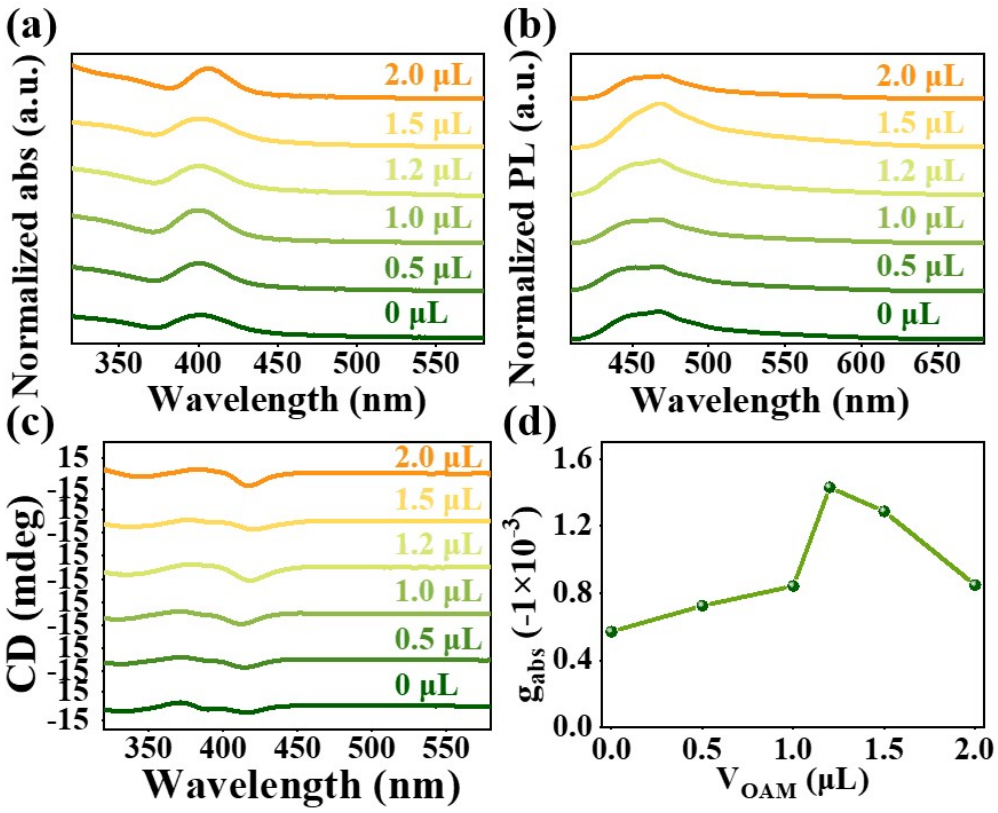

Figure S9. (a) UV absorption, (b) PL emission spectra and (c) CD spectra of (*R*-MPEA)$_4$AgBiBr$_8$ prepared by using different amounts of OAm. (d) Corresponding variation trend of g_{abs}-factor of these NBs synthesized in different volumes of OAm.

To further understand the properties of these chiral NBs, we also conducted an investigation into the influence of OAm, an achiral long-chain ligand, on the chiral optical signals or asymmetric factors of the 2D (*R*-MPEA)$_4$AgBiBr$_8$ NBs. The results, depicted in **Figure S9**, revealed that the addition of an appropriate amount of OAm led to higher CD signals, whereas excessive or insufficient amounts of OAm resulted in weak CD signals. This phenomenon can be explained by considering the influence of OAm on the self-assembly and arrangement of the chiral components within the NBs.[1] The optimum amount of OAm facilitates the formation of a well-ordered chiral structure, maximizing the chiral optical signals. However, an excess or inadequate amount of OAm can disrupt the preferred arrangement of the chiral components, leading to a decrease in the chiral optical response.

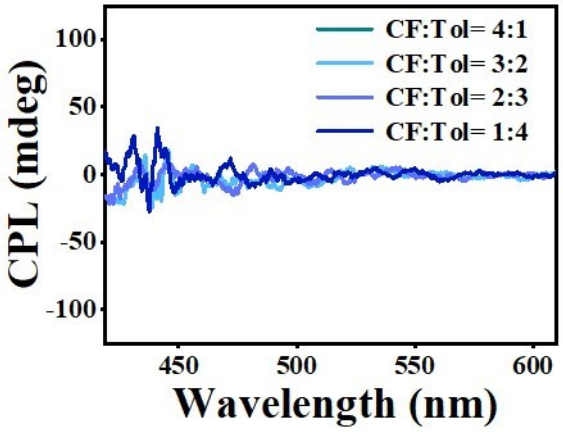

Figure S10. CPL spectra of $(R\text{-MPEA})_4AgBiBr_8$.

We conducted room-temperature circularly polarized luminescence (CPL) testing of $(R\text{-MPEA})_4AgBiBr_8$ solution. However, as depicted in **Figure S10**, no detectable CPL peak was observed. It has been reported that detecting CPL signals in two-dimensional chiral perovskite NBs in solution at room temperature can be challenging due to their strong electron-photon coupling and significant nonradiative recombination, especially in colloidal solutions.[1]

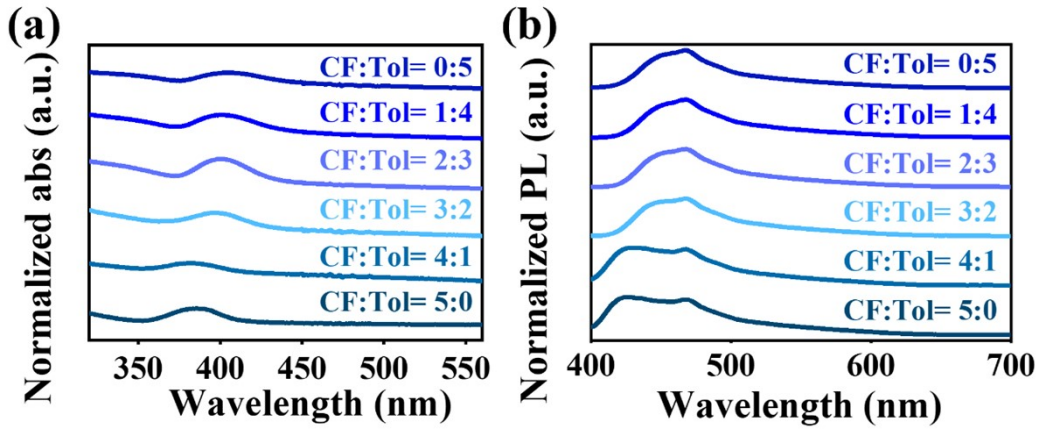

Figure S11. a) UV absorption spectra, b) PL emission spectra of 2D double $(R\text{-MPEA})_4AgBiBr_8$ perovskites synthesized at different volume ratios of chloroform (CF)/toluene (Tol).

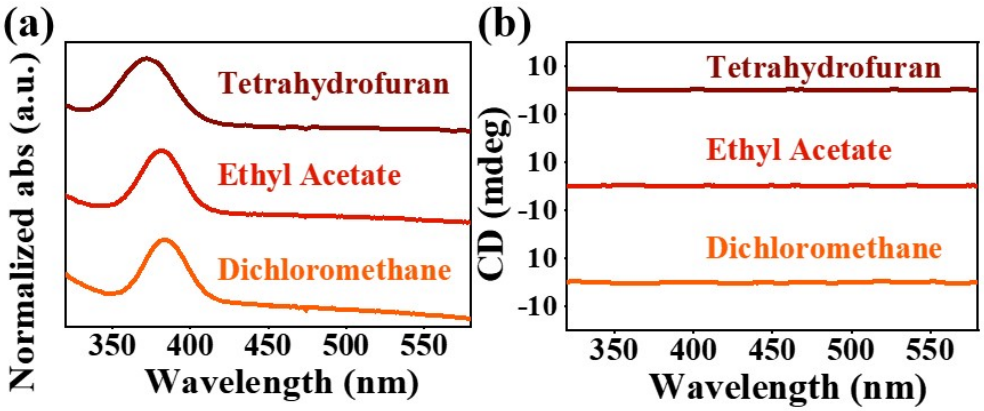

Figure S12. (a) The UV absorption spectra and (b) CD spectra of 2D double perovskite *R*-MPEA$_4$AgBiBr$_8$ obtained using different single antisolvents, namely tetrahydrofuran, ethyl acetate, and dichloromethane.

Similarly, other common antisolvents, including ethyl acetate, tetrahydrofuran, and chlorobenzene, were also unable to exhibit the expected CD signals, as displayed in **Figure S12**.

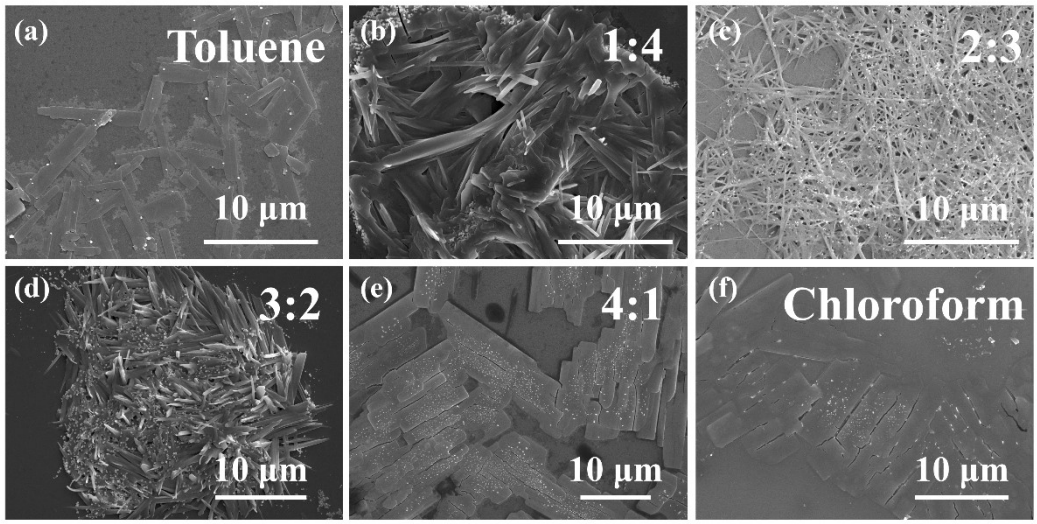

Figure S13. SEM images of 2D double perovskite *R*-MPEA$_4$AgBiBr$_8$ synthesized by using different volume ratios of chloroform/toluene mixtures as co-antisolvents: (a) toluene, (b) 1:4, (c) 2:3, (d) 3:2, (e) 4:1 and (f) chloroform.

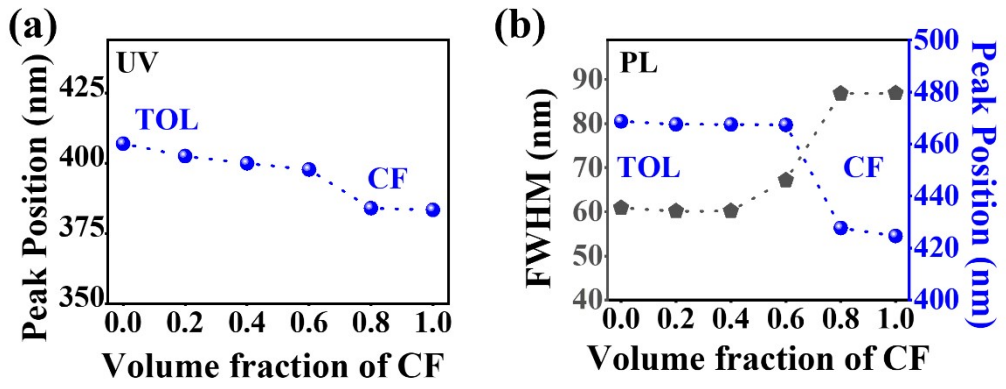

Figure S14. (a) The variation in UV absorbance and (b) PL emission peak position and FWHM of (*R*-MPEA)$_4$AgBiBr$_8$ NBs in different ratio of antisolvent.

By employing chloroform/toluene mixtures, it may serve a simply yet robust way to tune the chiroptical properties. When increasing the concentration of chloroform as a relative polar antisolvent, a slight blue shift in the peak position of both UV absorption and PL emission was observed, accompanied by a broadening of the emission peak, as illustrated in **Figures S11, and S14.** A similar blue-shift of absorbance and emission peak induced by quantum confinement can be attributed to an introduction of polar antisolvent, as reported in other perovskite materials previously.[10] Since the reaction kinetics were fast, some of the PL spectra reveal double peak or peak position shift due to the formation of nanocrystals with multiple thicknesses.[11]

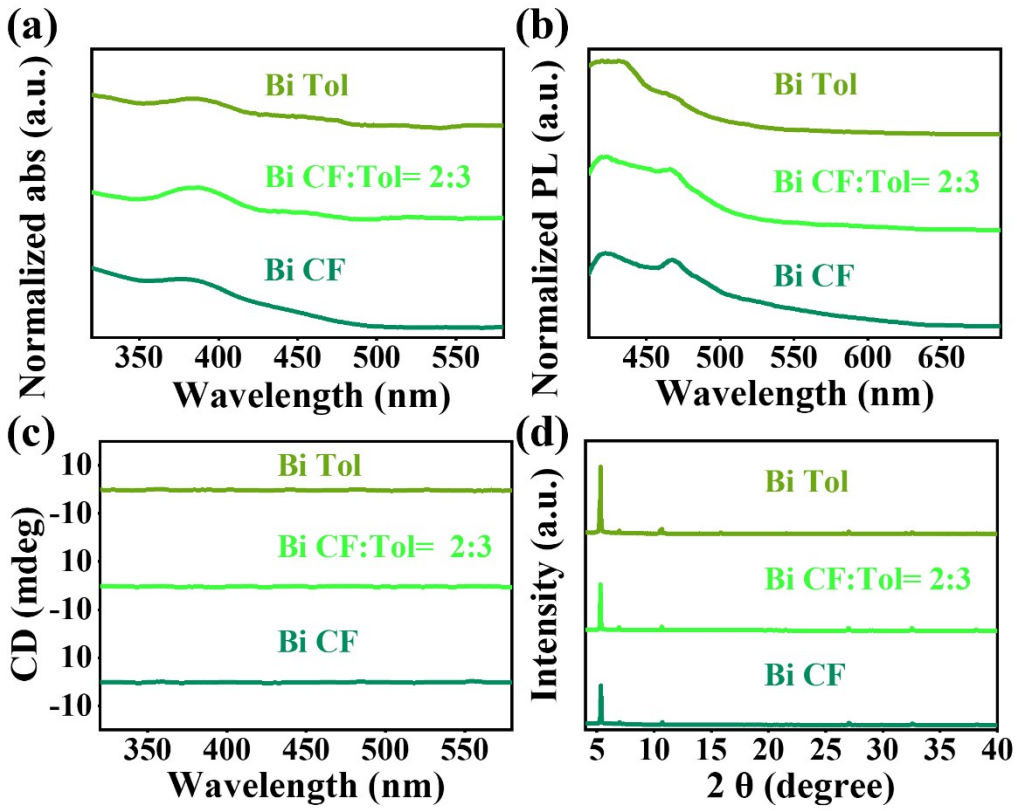

Figure S15. (a) The changes in UV absorbance spectrum, (b) PL emission spectrum, (c) CD spectrum and (d) corresponding XRD pattern of pure Bi perovskite compounds obtained using the same synthesis condition as 2D double (*R*-MPEA)$_4$AgBiBr$_8$ NBs, except the usage of AgBr in precursor solutions.

The absence of CD signals in the pure Bi-based perovskite compounds obtained under the same antisolvent and reaction conditions supports the notion that the chiral optical properties observed are specifically attributed to the coexistence of AgBr and $BiBr_3$ (**Figure S15**). This suggests that the chiral Ag-Bi double perovskite structure has indeed been successfully synthesized.

Table S2. 2D layer chiral perovskite in recently published literatures.

Chiral perovskite	A-site	Synthetic Method	Dimensionality	g_{abs}-Factor	Structure Modulations*	Ref.
(*R*-MPEA)$_4$AgBiBr$_8$	*R*-β-methylphenethylammonium(*R*-	LARP in co-antisolvent	2D	1.43×10^{-3} (R)	X-	This work

	MPEA)					
(*R/S*-$MBA_{0.75}PEA_{0.25})_2PbBr_4$	*S-/R-α*-methylbenzylamine(S-/R-MBA)	LARP in single antisolvent	2D	-3.8×10^{-3}(R) 3.1×10^{-3}(S)	A, B, X	*Adv. Optical Mater.*, 2023, 11, 2202290
(R/S-$MPEA)_2PbBr_4$	*S-/R*-b-methylphenethylammonium(*S-/R*-MPEA)	LARP in single antisolvent	2D	6.5×10^{-3} (*R*-MPEA NSs)	A	*J. Phys. Chem. Lett.*, 2021, 12, 2676
(*S*-$BrMBA)_2PbI_4$ with about 3.9% *S*-2-$MeBA^+$ as dopant in A site	(*S*)-(−)-2-methylbutylammonium(*S*-2-MeBA)) and (*S*)-(−)-4-bromo-α-methylbenzylammonium (*S*-BrMBA)	Cooling crystallization of single crystal	2D	1.88×10^{-4}	A	*J. Am. Chem. Soc.*, 2023, 145, 17831
(*R*-X-*p*-$mBZA)_2PbBr_4$ (X = H, F, Cl, Br)	*R*-α-methylbenzylamine*(R*-X-*p*-MBZ)	Cooling crystallization of single crystal	2D	(*R*-$mBZA)_2PbBr_4$ CD intensity around 15 mdeg	A	*Phys. Chem. Chem. Phys.*, 2020, 22, 17299
(*R/S*)-(BPEA)$FAPbBr_4·H_2O$	(*R/S*)-4-bromophenylethylaminium((*R/S*)-BPEA); formamidinium(FA)	Cooling crystallization of single crystal	2D	CD intensity around 10 mdeg	A	*Adv. Optical Mater.*, 2023, 2202726
[(*R/S*)-β-$MPA]_4AgBiI_8$	*S-/R*-β-methylphenethylammonium((*R/S*)-β-MPA)	Cooling crystallization of single crystal	2D	CD intensity around 20 mdeg	no-modulation*	*Angew. Chem.* 2021, 133, 8496
[(*R/S*-$PPA)_4(IPA)_6Ag_2Bi_4I_{24}]·2H_2O$ and [(*R/S*-$PPA)_4(IPA)_6Ag_2Bi_4I_{24}]·2H_2O$	*R/S*–1-phenylpropylamine(*R/S*-PPA); isopentylamine(IPA); n- n-butylamin(BA)	Cooling crystallization of single crystal	2D	3×10^{-4}	A	*Adv. Funct. Mater.*, 2023, 2214660

0-P, 1-PR, 2-PR(Mn0.2), 3-PR(Mn0.5), and 4-PR(Mn0.8)	R-(+)-β-methylphenethylamine; (R-(+)-β-$C_9H_{13}N$)	Cooling crystallization of single crystal	2D	No study	B	*J. Phys. Chem. Lett.*, 2021, 12, 12129−12134
(*R/S*-3AP)$_4$AgBiBr$_{12}$	(*R/S*)-3-aminopyrrolidine(*R/S*-3AP)	Cooling crystallization of single crystal	2D	CD intensity lower than 15 mdeg	no-modulation	*ACS Appl. Mater. Interfaces*, 2022, 14, 39451

*"structure modulations" means the structure modulations of A B or X-site, which were denoted as "A", "B", "X" in the table. *"no-modulation" means no modulations in perovskites structure.

To our knowledge, the strategy of modulating chiral perovskite through co-antisolvent is the first report. Besides, the g-factor we achieved is also comparable to those of the lead-based chiral perovskites. In short, this strategy has only been studied in the field of chiral 2D double perovskites, and is expected to be further explored in other fields of chiral perovskites.

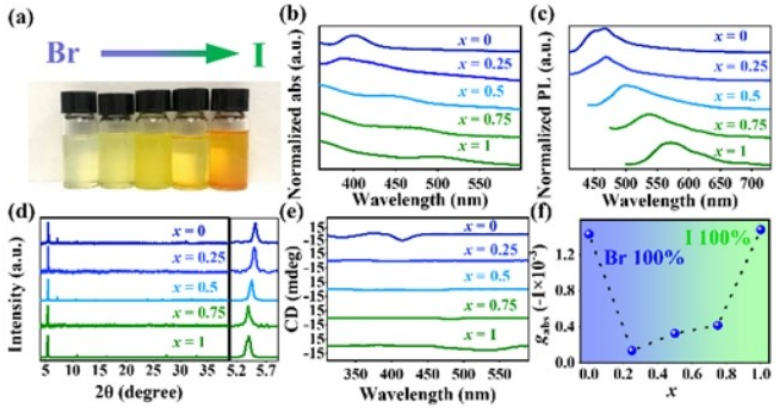

Figure S16. (*R*-MPEA)$_4$AgBiBr$_{8-8x}$I$_{8x}$ with different iodine contents. (a) Digital photos of colloidal solutions with different iodine contents under sunlight. (b) UV absorption spectra, (c) PL emission spectra, (d) XRD patterns, (e) CD spectra and (f) g_{abs}-factor values at maximum CD peak of (*R*-MPEA)$_4$AgBiBr$_{8-8x}$I$_{8x}$.

References:

1. H. Ren, Y. Wu, C. Wang and Y. Yan, *J. Phys. Chem. Lett.*, 2021, **12**, 2676-2681.
2. G. K. Long, R. Sabatini, M. I. Saidaminov, G. Lakhwani, A. Rasmita, X. G. Liu, E. H. Sargent and W. B. Gao, *Nat. Rev. Mater.*, 2020, **5**, 423-439.
3. X. Wang, K. Li, H. Xu, N. Ali, Y. Wang, Q. Shen and H. Wu, *Chem. Commun.*, 2020, **56**, 7917-7920.
4. L. He, S. Pan, Z. Lin and J. Peng, *ACS Appl. Nano Mater.*, 2019, **2**, 7910-7915.
5. F. Locardi, M. Cirignano, D. Baranov, Z. Dang, M. Prato, F. Drago, M. Ferretti, V. Pinchetti, M. Fanciulli, S. Brovelli, L. De Trizio and L. Manna, *J. Am. Chem. Soc.*, 2018, **140**, 12989-12995.
6. Y. Bekenstein, J. C. Dahl, J. Huang, W. T. Osowiecki, J. K. Swabeck, E. M. Chan, P. Yang and A. P. Alivisatos, *Nano Lett.*, 2018, **18**, 3502-3508.
7. F. Locardi, M. Cirignano, D. Baranov, Z. Dang, M. Prato, F. Drago, M. Ferretti, V. Pinchetti, M. Fanciulli and S. Brovelli, *J. Am. Chem. Soc.*, 2018, **140**, 12989-12995.
8. Z. Dang, J. Shamsi, F. Palazon, M. Imran, Q. A. Akkerman, S. Park, G. Bertoni, M. Prato, R. Brescia and L. Manna, *ACS Nano*, 2017, **11**, 2124-2132.
9. D. F. Wu, Y. Tao, Y. Y. Huang, B. J. Huo, X. S. Zhao, J. Y. Yang, X. F. Jiang, Q. Huang, F. Dong and X. S. Tang, *J. Catal.*, 2021, **397**, 27-35.
10. L. Z. He, S. Pan, Z. Q. Lin and J. Peng, *ACS Appl. Nano Mater.*, 2019, **2**, 7910-7915.
11. Y. Bekenstein, B. A. Koscher, S. W. Eaton, P. D. Yang and A. P. Alivisatos, *J. Am. Chem. Soc.*, 2015, **137**, 16008-16011.